

Thermal Dynamic Phase Transition of Reissner-Nordström Anti-de Sitter Black Holes on Free Energy Landscape

Ran Li,^{a,b} Kun Zhang,^c Jin Wang^{1d}

^a*Department of Physics, Henan Normal University, Xinxiang 453007, China*

^b*Department of Chemistry, State University of New York at Stony Brook, Stony Brook, NY 11794-3400, USA*

^c*State Key Laboratory of Electroanalytical Chemistry, Changchun Institute of Applied Chemistry, Chinese Academy of Sciences, Changchun, China, 130022*

^d*Department of Physics and Astronomy, State University of New York at Stony Brook, Stony Brook, NY 11794-3400, USA*

E-mail: liran@htu.edu.cn, zhangkun@ciac.ac.cn,
jin.wang.1@stonybrook.edu

ABSTRACT: We explore the thermodynamics and the underlying kinetics of the van der Waals type phase transition of Reissner-Nordström anti-de Sitter (RNAdS) black holes based on the free energy landscape. We show that the thermodynamic stabilities of the three branches of the RNAdS black holes are determined by the underlying free energy landscape topography. We suggest that the large (small) RNAdS black hole can have the probability to switch to the small (large) black hole due to the thermal fluctuation. Such a state switching process under the thermal fluctuation is taken as a stochastic process and the associated kinetics can be described by the probabilistic Fokker-Planck equation. We obtained the time dependent solutions for the probabilistic evolution by numerically solving Fokker-Planck equation with the reflecting boundary conditions. We also investigated the first passage process which describes how fast a system undergoes a stochastic process for the first time. The distributions of the first passage time switching from small (large) to large (small) black hole and the corresponding mean first passage time as well as its fluctuations at different temperatures are studied in detail. We conclude that the mean first passage time and its fluctuations are related to the free energy landscape topography through barrier heights and temperatures.

¹Corresponding author

Contents

1	Introduction	1
2	Thermodynamics of RNAdS black hole	4
2.1	Thermodynamic characterization	4
2.2	Free energy landscape	5
2.3	Thermodynamic stability of emergent phases, phase transitions and phase diagram	7
3	Fokker-Planck equation governing the probabilistic evolution on the free energy landscape	8
4	Kinetics and its fluctuations of black hole state switching dynamics	11
5	Conclusion	17

1 Introduction

Hawking’s original derivation of blackbody radiation from a collapsing black hole [1] revealed the thermal nature of black holes. This discovery established a close relationship between gravity, thermodynamics, and statistical physics. Since then, studying black hole from the thermodynamic and statistical physics viewpoint has attracted significant attention. Hut studied the phase transitions of charged black holes [2]. Davies found that Kerr-Newman black holes can undergo a second order phase transition at the point where the heat capacities are divergent [3]. By treating black hole as a state in the thermodynamic ensemble, Hawking and Page [4] studied the first order phase transition from thermal AdS space to the large AdS black hole at a certain critical temperature. More recently, the first order phase transition between the small and the large RNAdS black holes was studied by Chamblin et al [5–7]. By treating the cosmological constant as thermodynamic pressure and the black hole mass as enthalpy, Dolan also discovered the remarkable analogy between van der Waals liquid-gas system and RNAdS black hole in extended phase space [8, 9]. Kubiznak and Mann [10] showed the critical behavior of RNAdS black hole in fixed charge ensemble coincides exactly with that of van der Waals liquid-gas system.

The discovery of the anti-de Sitter/conformal field theory (AdS/CFT) correspondence [11–13] greatly promotes the studying of phase transition of black holes in AdS space. It is well known that, by AdS/CFT correspondence, Hawking-Page transition can be properly explained as the confinement/deconfinement transition in quantum chromodynamics (QCD) [14]. In particular, the analogy between AdS black holes and van der Waals liquid has been studied extensively, including the small-large black hole transition in modified

gravity and higher derivative gravity [15–25], Maxwell equal area rule of van der Waals type phase transition of charged AdS black hole [26, 27], quasinormal modes behavior near the phase transition points [28], van der Waals behavior of entanglement entropy in charged AdS black hole [29, 30], hairy black hole chemistry [31], Ruppeiner geometry [32–36], and black hole microstructure [37, 38]. One can refer to [39] for a comprehensive recent review of P-V criticality of charged AdS black holes.

In thermodynamics and statistical physics, system is considered to be made up of molecules, and the macroscopic properties can be determined by the degrees of freedoms from microscopic molecules. The liquid or gas or solid form of materials is in this sense a macroscopic emergent state. In general, for one certain system considered, there are many possible microscopic states. Each state has a different weight or probability to appear. These emergent states have larger weights which are associated with the thermodynamic free energy by the Boltzmann law. The free energy distributed in the whole state space forms a free energy landscape [40–42]. The free energy landscape can be characterized and studied by its dependence on the order parameters such as density in van der Waals liquid-gas system. It should be noted that the temperature can modulate the free energy landscape on the order parameter space. In this picture, the local stationary state, which is represented by the local basin (minimum) of the free energy landscape, can have the probability to switch to the global stationary state represented by the global basin (minimum) and vice versa. Then any state has a life time due to the chance of transition to other states. Notice that the thermal fluctuation is the reason behind the kinetics of this type of state switching.

In this work, inspired by the analogy of RNAdS black holes and van der Waals liquid system, we will go a few steps further and gain deeper understanding on this by studying the thermodynamics and the underling kinetics of the phase transition between the small and the large RNAdS black holes based on the free energy landscape. The free energy landscape formalism for the black hole system is formulated in the recent paper [43]. It has been applied to study the thermodynamics and the kinetics of Hawking-Page phase transitions in Einstein gravity and massive gravity [43].

The main assumptions to formulate the free energy landscape for black hole system are listed as follows [43]. From the thermodynamics and statistical physics viewpoint, a black hole should be treated as an emergent state of the microscopic degrees of freedom. The black hole horizon radius can be taken as the proper order parameter that describes the microscopic degrees of freedom. This point is different but related to the viewpoint that the number density of the black hole molecules is the order parameter to measure the microscopic degrees of freedom [37, 38]. It is further proposed that, at the specific temperature, there exists a series of black hole spacetimes, with the horizon radius ranging from zero to infinity. For the small/large RNAdS black hole phase transition, these spacetime states include the small, the large, the intermediate black holes, and all the transient states during the phase transition. These spacetime states compose the canonical ensemble we are considering. The free energy landscape is formulated by specifying every spacetime in the ensemble a Gibbs free energy. In the present case, this can be achieved by generalizing the on-shell Gibbs free energy for the three branches of RNAdS black holes to all

spacetime states. The generalized Gibbs free energy, which can be expressed as a function of the order parameter and the ensemble temperature, is off-shell because the transient spacetime states are not the solutions to the Einstein equations. Using the Gibbs free energy topography, the emergence of the phases and the associated phase transition can be analyzed. Furthermore, by adjusting the ensemble temperatures, we can also analyze the phase diagram and explore the thermodynamic stability.

For the underlying kinetics of black hole phase transition, it is proposed that the stochastic dynamics of black hole phase transition under thermal fluctuations can be studied by using the associated probabilistic Fokker-Planck equation on the free energy landscape [44–48]. In this regard, due to the thermal fluctuation, a small (large) black hole state can have the chance to switch to a different state such as large (small) black hole state through the thermal free energy barrier crossing process. By solving the Fokker-Planck equation with proper boundary condition, we can obtain the stationary probability distribution of black hole states at different temperatures as well as the mean first passage time of the kinetics process from the small black hole to the large black hole and vice versa. On the free energy landscape, kinetics are closely related to the shape of the free energy landscape when varying the temperatures [45–48]. We further study the statistical fluctuations and distributions of the kinetics at various temperatures. Again the landscape topography is important for characterizing the behaviors of the fluctuations in kinetics.

In principle, the free energy landscape formalism can be applied to study any kind of phase transition of black hole system. In [43], it has been applied to study the Hawking-Page phase transitions in Einstein gravity and in massive gravity. This provides us significant insights into understanding the underlying thermodynamics and kinetics of the Hawking-Page phase transition. In the present work, our aim is to apply this formalism to study the van der Waals type phase transition in RNAdS black holes. This type of phase transition is very different from the Hawking-Page transition and of very important significance in studying the microstructures of AdS black holes [49–54]. It should be noted that our method in this work is also different from that used in [43]. In this work, we study the kinetics of the first passage process by numerically solving the Fokker-Planck equation. In this way, we can obtain not only the mean first passage time and its statistical fluctuation but also the probabilistic evolution of spacetime state and the distribution of the first passage time. In [43], the analytical expressions for the mean first passage time and its fluctuation were derived, from which the kinetics of the first passage process is studied. In this sense, this work provides an alternative method to study the kinetics and its distribution of the phase transition in the black hole system.

This paper is arranged as follows. In section II, we explore the thermodynamics and phase transition of RNAdS black hole through free energy landscape. In section III, we study the Fokker-Planck equation on the free energy landscape for quantifying the probabilistic evolution of the underlying stochastic dynamics. The time dependent probabilistic evolution solutions are also obtained by numerically solving Fokker-Planck equation with the reflecting boundary conditions. In section IV, we present the numerical results of the distributions of first passage time switching from small (large) to large (small) black hole phases and the corresponding mean first passage time and its fluctuations at different

temperatures. The conclusion and discussion are presented in the last section.

2 Thermodynamics of RNAdS black hole

2.1 Thermodynamic characterization

We start with the metric of RNAdS black hole, which describes the spherically symmetric charged black hole solution to Einstein-Maxwell action with negative cosmological constant [55]. The line element is given by ($G = 1$ units)

$$ds^2 = - \left(1 - \frac{2M}{r} + \frac{Q^2}{r^2} + \frac{r^2}{L^2} \right) dt^2 + \left(1 - \frac{2M}{r} + \frac{Q^2}{r^2} + \frac{r^2}{L^2} \right)^{-1} dr^2 + r^2 d\Omega^2, \quad (2.1)$$

where M is the mass, Q is the charge, and $L = \sqrt{\frac{-3}{\Lambda}}$ is the AdS curvature radius with Λ being the cosmological constant.

The event horizon is determined by the largest root of the equation

$$f(r) = 1 - \frac{2M}{r} + \frac{Q^2}{r^2} + \frac{r^2}{L^2} = 0. \quad (2.2)$$

The mass of black hole can be expressed in terms of the horizon radius r_+ as

$$M = \frac{r_+}{2} \left(1 + \frac{r_+^2}{L^2} + \frac{Q^2}{r_+^2} \right). \quad (2.3)$$

The Hawking temperature is given by

$$T_H = \frac{1}{4\pi} f'(r)|_{r=r_+} = \frac{1}{4\pi r_+} \left(1 + \frac{3r_+^2}{L^2} - \frac{Q^2}{r_+^2} \right). \quad (2.4)$$

In the case of an asymptotically AdS black hole in four dimensions, one can relate the thermodynamic pressure to the cosmological constant as suggested by Doaln et al [8, 9]

$$P = \frac{3}{8\pi} \frac{1}{L^2}. \quad (2.5)$$

Replacing the cosmological constant by thermodynamic pressure in Eq.(2.4), Hawking temperature can be rewritten as

$$T_H = \frac{1}{4\pi r_+} \left(1 + 8\pi P r_+^2 - \frac{Q^2}{r_+^2} \right). \quad (2.6)$$

There exists a critical pressure $P_c = \frac{1}{96\pi Q^2}$, above which black hole temperature T_H is a monotonic function of black hole radius r_+ , while below which black hole temperature T_H have the local minimal and local maximum value. In Fig.1, we have depicted the black hole temperature as a function of black hole radius r_+ when $P < P_c$ (left pannel) and $P > P_c$ (right pannel).

When $P < P_c$, the local minimal and local maximum values of black hole temperature are determined by equation

$$\frac{\partial T_H}{\partial r_+} = 0, \quad (2.7)$$

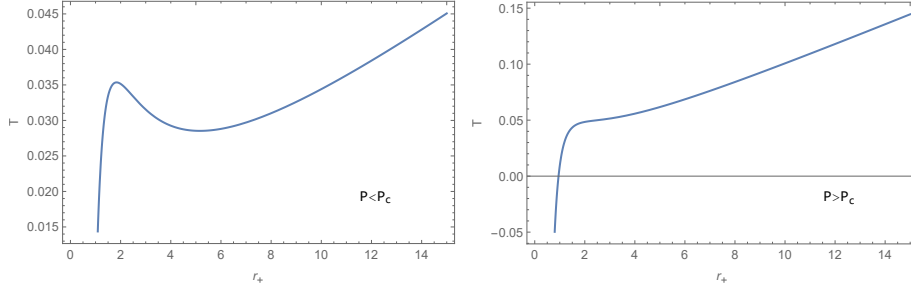


Figure 1. Black hole Temperature T_H as a function of event horizon radius r_+ when $P < P_c$ (left pannel) and $P > P_c$ (right pannel).

which gives us the solutions

$$r_{min/max} = \left[\frac{1 \pm \sqrt{1 - 96\pi PQ^2}}{16\pi P} \right]^{1/2}. \quad (2.8)$$

when substituting back to Eq.(2.6), one can get the local minimal and local maximum values of black hole temperature which are respectively given by

$$T_{min/max} = \frac{2\sqrt{P} \left(1 - 32\pi PQ^2 \pm \sqrt{1 - 96\pi PQ^2} \right)}{\sqrt{\pi} \left(1 \pm \sqrt{1 - 96\pi PQ^2} \right)^{3/2}}. \quad (2.9)$$

When $T_{min} < T_H < T_{max}$, there exists three branches of black hole solution (i.e. small, intermediate, and large black hole). The intermediate solution is unstable. Similar to the van der Waals liquid-gas system, there is a first order phase transition from the small black hole to the large black hole.

2.2 Free energy landscape

As discussed in the Introduction, we consider the canonical ensemble at the specific temperature T which is composed by a series of black hole spacetimes with an arbitrary horizon radius. The on-shell Gibbs free energy for the three branches of RNAdS black hole can be given by the thermodynamic relationship $G = M - T_H S$ or calculated directly from the Euclidean action [9]. Replacing the Hawking temperature T_H by the ensemble temperature T in the on-shell Gibbs free energy expression, we can define the generalized off-shell Gibbs free energy for the transient black hole state, which is given by

$$G = M - TS = \frac{r_+}{2} \left(1 + \frac{8}{3}\pi P r_+^2 + \frac{Q^2}{r_+^2} \right) - \pi T r_+^2. \quad (2.10)$$

This Gibbs free energy should be considered as the generalized canonical free energy, where the horizon radius r_+ can take all values from zero to infinity because r_+ is taken as the order parameter to describe the microscopic degrees of freedom [43]. This type of the generalized free energy has been applied to investigate and understand the physical process of the phase transitions in the Schwarzschild black holes [56, 57]. In this way, we can then

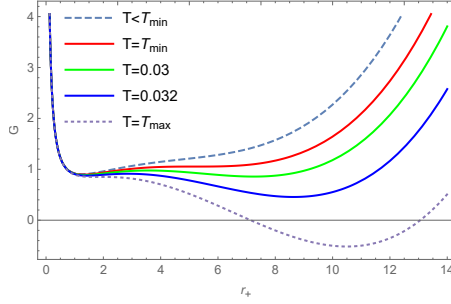


Figure 2. Gibbs free energy as a function of r_+ for $P < P_c$ with different temperatures.

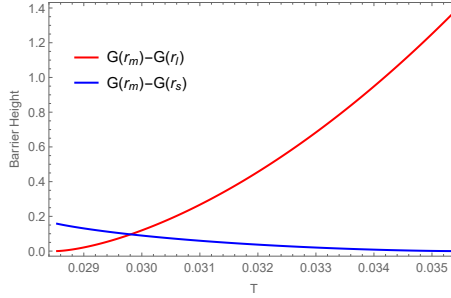


Figure 3. Barrier height as a function of temperature T . The red line represents the barrier height between the intermediate black hole and the large black hole, while the blue line represents the barrier height between the intermediate black hole and the small black hole.

formulate the free energy landscape for the RNAdS black holes. Thus we can quantify the free energy landscape by plotting the free energy as a function of black hole radius r_+ as shown in Fig. 2 for different temperatures. In the plot, $P = 0.4P_c$, $Q = 1$, $T_{min} = 0.0285$, and $T_{max} = 0.0354$.

It can be seen when $T_{min} < T < T_{max}$ the Gibbs free energy has double basin (well) shape. In this case, the Gibbs free energy has three local extremals (two stable and one unstable), which are determined by the equation

$$\frac{\partial G}{\partial r_+} = \frac{1}{2} + 4\pi P r_+^2 - \frac{Q^2}{2r_+^2} - 2\pi T r_+ = 0. \quad (2.11)$$

This is just the equation for the black hole temperature T_H . By solving this equation for r_+ , one can get the lengthy expressions of the radii for the small, large, and intermediate black holes. We denote them as r_s , r_m , and r_l , respectively, which are determined by T , P , and Q . The intermediate black hole which corresponds to the maximum value of the Gibbs free energy is unstable. The small and large black holes are all locally stable, and the thermodynamically stable black hole has the minimal Gibbs free energy.

Gibbs free energy for the the small, large, and intermediate black holes are given by

$$G_{s/m/l} = \frac{r_{s/m/l}}{4} - \frac{2}{3}\pi P r_{s/m/l}^3 + \frac{3}{4} \frac{Q^2}{r_{s/m/l}}. \quad (2.12)$$

The free energy landscape topography quantified by the free energy barrier heights from the small black hole to the large black hole and from the large black hole to the small black hole are plotted in Fig.3. It is obvious that they are all monotonic functions of the black hole temperature. When temperature increases, the free energy barrier from small black hole state to the large black hole state decreases while the free energy barrier from large black hole state to the small black hole state increases. This is consistent with the free energy landscape as a function of black hole radius at varying temperatures as shown in Fig.2.

2.3 Thermodynamic stability of emergent phases, phase transitions and phase diagram

There exists a transition temperature determined by the Gibbs free energies of the large black hole and small black hole are equal. The transition temperature should be determined by the following equations

$$\begin{aligned} \frac{1}{2} + 4\pi Pr_s^2 - \frac{Q^2}{2r_s^2} - 2\pi Tr_s &= 0, \\ \frac{1}{2} + 4\pi Pr_l^2 - \frac{Q^2}{2r_l^2} - 2\pi Tr_l &= 0, \\ \frac{r_s}{4} - \frac{2}{3}\pi Pr_s^3 + \frac{3}{4}\frac{Q^2}{r_s} &= \frac{r_l}{4} - \frac{2}{3}\pi Pr_l^3 + \frac{3}{4}\frac{Q^2}{r_l}. \end{aligned} \quad (2.13)$$

In Fig.4, we have plotted the transition temperature as well as $T_{min/max}$ as a function of pressure P . These curves separate the $P - T$ plane into four regions. In the regions of below the black line and above the blue line, there is only one black hole solution, and it is always thermodynamic stable. In the middle region, there are three black hole solutions as discussed above. The red line represents the transition temperature, where the free energies for the small black hole and the large black hole are equal, i.e. the red line represents the coexistence curve that the small and the large black hole phases coexists. In the region between red line and black line, the free energy of small black hole is less than the free energy of the large black hole, while in the region between red line and blue line this relation is inverted. So, we can conclude that the small black hole is thermodynamic stable in the pink region and the large black hole is thermodynamic stable in the yellow region. However, from the ensemble viewpoint, the stable black hole states still have the probability switching into the unstable black hole state under the thermal fluctuations. We will study this probability by studying the kinetics process described by Fokker-Planck equation and Langevin equation in the following sections.

In Fig.4, we provided the thermodynamic phase diagram by plotting the transition temperature as well as $T_{min/max}$ as a function of pressure P . These curves separate the $P - T$ plane into four thermodynamic phase regions. In the phase regions of below the black line and above the blue line, there is only one black hole solution, and it is always thermodynamic stable. In the middle phase region, there are three black hole solutions as discussed above. The red line represents the transition temperature, where the free energies for the small black hole and the large black hole are equal, i.e. the red line

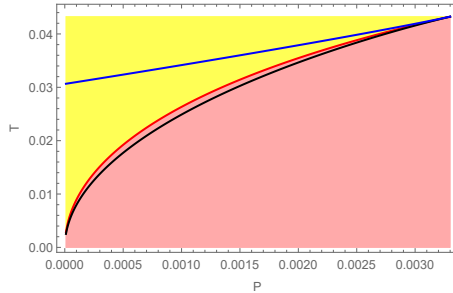


Figure 4. Phase diagram of RNAdS black holes. The blue, black, and red lines are the plots of T_{max} , T_{min} , and T_{trans} as a function of pressure P . In these plots, the range of P is from 0 to the critical pressure P_c . The small and large black holes are thermodynamically stable in pink and yellow regions, respectively.

represents the coexistence curve that the small and the large black hole phases coexists in equal probability. In the phase region between the red line and the black line, the free energy of the small black hole is less than the free energy of the large black hole, while in the phase region between the red line and the blue line this relation is reversed. Therefore, we can conclude that the small black hole is thermodynamically stable in the phase region between the red line and the black line and the large black hole is thermodynamically stable in the phase region between the red line and the blue line. However, from the ensemble viewpoint, the stable black hole states still have the chance of switching into other black hole state due to the presence of the thermal fluctuations. We will examine this by studying the corresponding kinetics process described by the probabilistic Fokker-Planck equation in the following sections.

The secondary derivative of Gibbs free energy is given by

$$\frac{\partial^2 G}{\partial r_+^2} = 8\pi P r_+ + \frac{Q^2}{r_+^3} - 2\pi T. \quad (2.14)$$

By solving the equation $\frac{\partial^2 G}{\partial r_+^2} = 0$ together with Eq.(2.11), one can also determine the local minimal and local maximum values of temperature which are given by Eq.(2.9).

3 Fokker-Planck equation governing the probabilistic evolution on the free energy landscape

In this section, we will discuss the transition state theory of black hole state switching or phase transition by treating black hole as a state in extended phase space. As shown in the last section, we know that Gibbs free energy landscape as a function of black hole radius exhibits double basin (well) shape when $T_{min} < T < T_{max}$. The two local minima correspond to the small and the large black holes respectively. One naturally regards the black hole radius as the reaction coordinate or order parameter.

From now on, we use the symbol r to denote the black hole radius r_+ for the sake of simplicity. In the formalism of free energy landscape, the Gibbs free energy $G(r)$ is a function of the order parameter r , where r denotes the black hole radius. Our aim

is to study the evolution of the system under the thermal fluctuation. The probability distribution of these states evolving in time should be a function of the order parameter r (black hole radius) and time t . Thus, the probability distribution of spacetime state in the ensemble is denoted by $\rho(r, t)$. So we firstly write down the corresponding Fokker-Planck probabilistic evolution equation.

The Fokker-Planck equation for the probabilistic evolution on the free energy landscape is explicitly given by [44–48]

$$\frac{\partial \rho(r, t)}{\partial t} = D \frac{\partial}{\partial r} \left\{ e^{-\beta G(r)} \frac{\partial}{\partial r} \left[e^{\beta G(r)} \rho(r, t) \right] \right\}. \quad (3.1)$$

In the above equation, the inverse temperature is $\beta = 1/kT$ and the diffusion coefficient is $D = kT/\zeta$ with k being the Boltzman constant and ζ being dissipation coefficient. Without loss of generality, we will take $k = \zeta = 1$ in the following.

In order to solve the Fokker-Planck equation, two types of boundary conditions should be imposed at the boundaries of computational domain depending on the question we consider. We list the boundary conditions at $r = r_0$ for example.

- Reflecting boundary condition:

$$e^{-\beta G(r)} \frac{\partial}{\partial r} \left[e^{\beta G(r)} \rho(r, t) \right] \Big|_{r=r_0} = 0. \quad (3.2)$$

It is equivalent to

$$\beta G'(r) \rho(r, t) + \rho'(r, t) \Big|_{r=r_0} = 0. \quad (3.3)$$

- Absorbing boundary condition:

$$\rho(r_0, t) = 0. \quad (3.4)$$

In this section, we study the time evolution of probability of state distribution in extended phase space by imposing the reflecting boundary condition at the points where Gibbs free energy is divergent, i.e. $r = 0$ and $r = +\infty$. However, in practice numerical computation, we typically set the reflecting boundary condition at $r = 0.1$ and $r = 12$ in order to avoid the numerical instability. The reflecting boundary condition will preserve the normalization of probability distribution. We choose the initial condition as

$$\rho(r, 0) = \frac{1}{\sqrt{\pi a}} e^{-(r-r_i)^2/a^2}, \quad (3.5)$$

with the parameter $a = 0.1$. This Gaussian wave packet is a good approximation of δ -distribution in numerical computation process. It should be noted that the initial wave pocket is normalized. We have checked that the normalization of probability distribution is preserved in the evolution process. We take $r_i = r_s$ or $r_i = r_l$ as the initial condition of system, which means that the system initially is either in small or large black hole state.

The time dependent behaviors of the probability distribution of the black holes in extended phase space at different temperatures are plotted in Fig.5 and Fig.6. In Fig.5

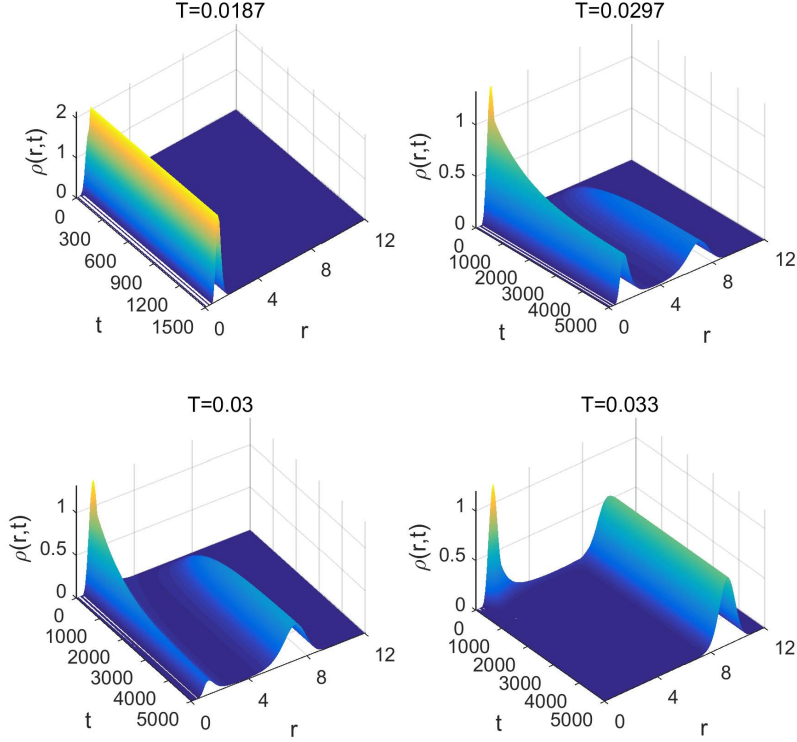


Figure 5. The distributions of probability $\rho(r, t)$ at different temperatures $T = 0.0187, 0.0297, 0.03$ and 0.033 . The initial wave packet is located at the small black hole representation.

and Fig.6, the initial probability distributions are Gaussian wave pockets located at the small and the large black hole radii respectively. In these plots, it can be observed that, the probability distribution of the black hole states reaches a quasi-stationary distribution very quickly at very early time, and then the final stationary distribution will be saturated at long time limit. It is shown the peak shape of the initial distribution will become smooth distribution within the free energy basin (well) where the initial wave packet locates. This quasi-stationary distributions of probability at very early time are only determined by the local free energy basin (well), and are not affected by the existence of the other free energy basin (well). Then the smooth quasi-stationary distributions will spread out to the other free energy basin (well) along the time.

The final stationary distributions are determined by $\rho_{st}(r) \propto e^{-G(r)/T}$, which can be obtained easily from the Fokker-Planck equation by setting $\frac{\partial \rho(r,t)}{\partial t} = 0$. This is consistent with the Boltzmann relationship between the free energy and the equilibrium probability distribution. Therefore, the stationary distribution from the long time evolution reaches the equilibrium probability. The thermodynamic stable state is then determined by the maximum of the final stationary distribution. However, on the free energy landscape theory, black hole state can have the chance of escape from one state to another due to the presence of thermal fluctuations.

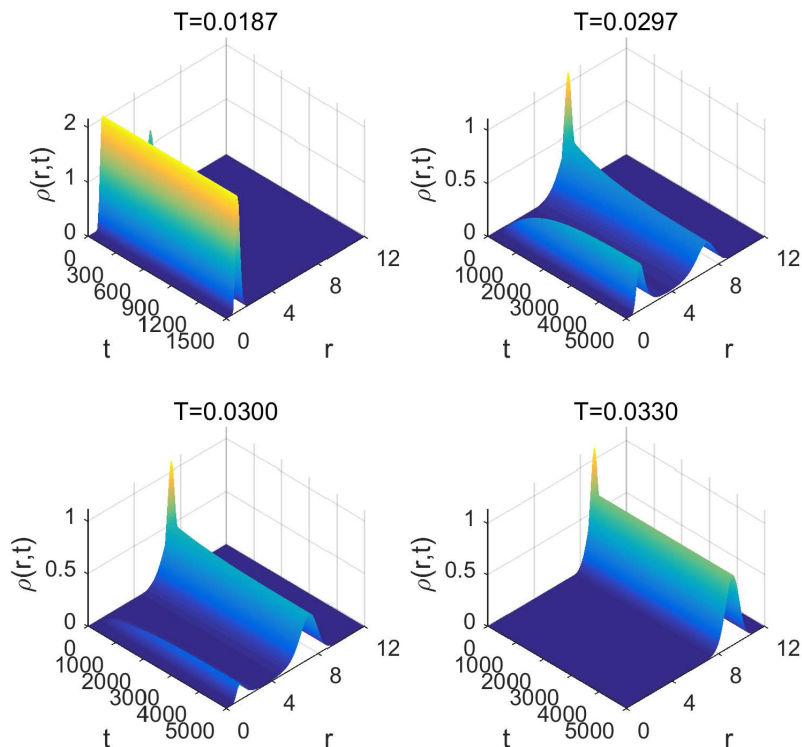


Figure 6. The distributions of probability $\rho(r, t)$ at different temperatures $T = 0.0187, 0.0297, 0.03$ and 0.033 . The initial wave packet is located at the large black hole representation.

4 Kinetics and its fluctuations of black hole state switching dynamics

In this section, we will study the kinetics by first passage process from one black hole state to another black hole state on the underlying free energy landscape. First passage time is a very important quantity in transition state theory, which can be defined as the time required for the state of the black hole to reach the intermediate transition state (represented by free energy barrier top) of the black hole for the first time in the present case. The mean first passage time defines an average timescale for a stochastic event to first occur.

Firstly, let us consider the first passage time of system from the small black hole state to the large black hole state. We denote the distribution of first passage times by $F_p(t)$ and define $\Sigma(t)$ to be the probability that the state of black hole has not made a first passage by time t . The distributions $F_p(t)$ and $\Sigma(t)$ are related by

$$F_p(t) = -\frac{d\Sigma(t)}{dt} . \quad (4.1)$$

According to the definition, $\Sigma(t)$ is defined as the probability of black hole being in the

system at time t . So we have

$$\Sigma(t) = \int_0^{r_m} \rho(r, t) dr . \quad (4.2)$$

It is obvious that $F_p(t)dt$ is the probability that a small black hole state passes through the intermediate transition state of the black hole (free energy barrier top) for the first time in the time interval $(t, t + dt)$. Suppose there is a perfect absorber placed at the site r_m (transition state at the free energy barrier top). If the state of a black hole makes the first passage under the thermal fluctuation, this black hole state leaves the system. In this setup, we have made the assumption that the time taken from the intermediate transition state of the black hole to the large black hole state is much smaller than the first passage time. The normalization of the probability distribution will not be preserved in this case. Therefore, at very late time, the probability of the black hole still in the system becomes zero, i.e. $\Sigma(r, t)|_{t \rightarrow +\infty} = 0$.

By substituting Eq.(4.2) into eq.(4.1), and using the Fokker-Planck equation (3.1), one can get

$$\begin{aligned} F_p(t) &= -\frac{d}{dt} \int_0^{r_m} \rho(r, t) dr \\ &= -\int_0^{r_m} \frac{\partial}{\partial t} \rho(r, t) dr \\ &= -D \int_0^{r_m} \frac{\partial}{\partial r} \left\{ e^{-\beta G(r)} \frac{\partial}{\partial r} \left[e^{\beta G(r)} \rho(r, t) \right] \right\} dr \\ &= -D e^{-\beta G(r)} \frac{\partial}{\partial r} \left[e^{\beta G(r)} \rho(r, t) \right] \Big|_0^{r_m} \\ &= -D \frac{\partial}{\partial r} \rho(r, t) \Big|_{r=r_m} , \end{aligned} \quad (4.3)$$

where we have imposed the reflecting boundary condition at $r = 0$ and the absorbing boundary condition at $r = r_m$ (transition state at free energy barrier top). By solving Fokker-Planck equation with the initial condition and boundary conditions, we can get the time distributions of first passage times. It is usually difficult to solve the combined initial value and boundary value problem described by Eqs.(3.1)-(3.5). So we also invoke the numerical method.

In Fig.7, we display the distribution of first passage time at different temperatures as a function of temperature. The initial distributions are Gaussian wave packets located at the small black hole state. These plots for different temperatures show the general behavior of the first passage time distribution. It can be observed there is a single peak in the first passage time distribution. This implies a considerable fraction of the first passage events occur at short times before the first passage time distribution has attained its exponential decay form. When the temperature increases, the peak becomes more sharper. In addition, the location of the peak moves to the left. This is because the barrier height from the small black hole state to the large black hole state through the intermediate transition state decreases when the temperature increases as observed from Fig.3. This makes the black

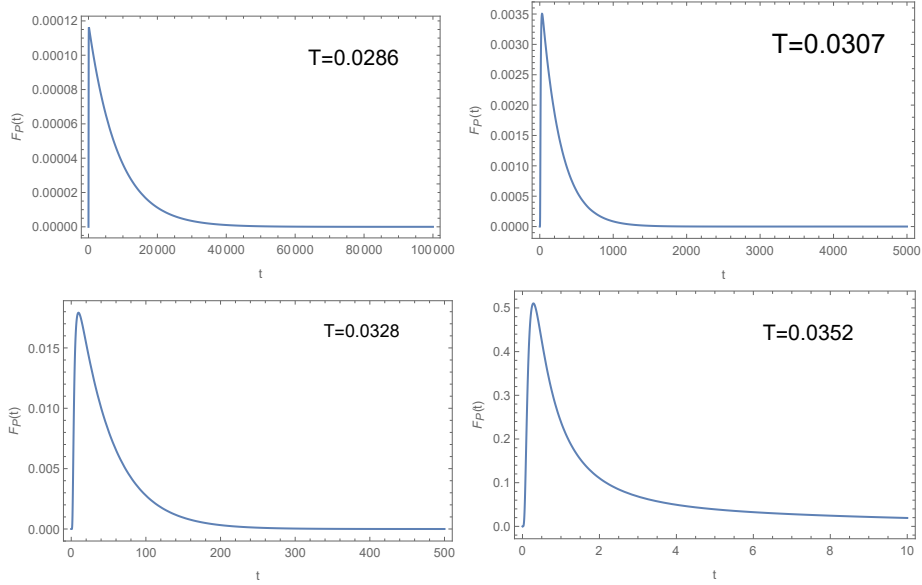


Figure 7. The distributions of first passage time $F_p(t)$ from small to large black hole state transition at different temperatures. The initial distribution is Gaussian wave packet located at the small black hole state.

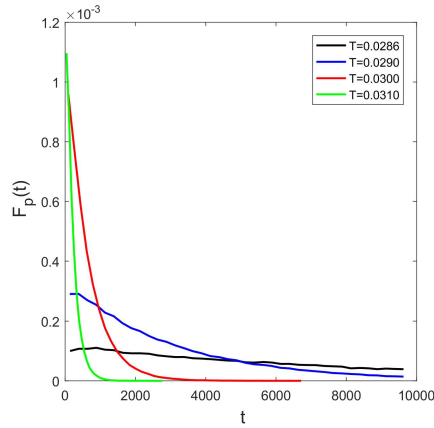


Figure 8. The tail parts of time distributions $F_p(t)$ from small to large black hole state transition at different temperatures.

hole state easier to go across the barrier under the thermal fluctuation. The tail part of the distribution indicates the fluctuation in kinetics. The longer the tail of the distribution is, the bigger the fluctuations in kinetics are. In Fig.8, the tail parts of time distributions $F_p(t)$ at different temperatures are plotted in one panel. It can be seen the fluctuation will become smaller at higher temperature. This point will be further confirmed by directly computing the fluctuation of first passage time in the following.

With the time distributions, we can calculate the mean first passage time and its

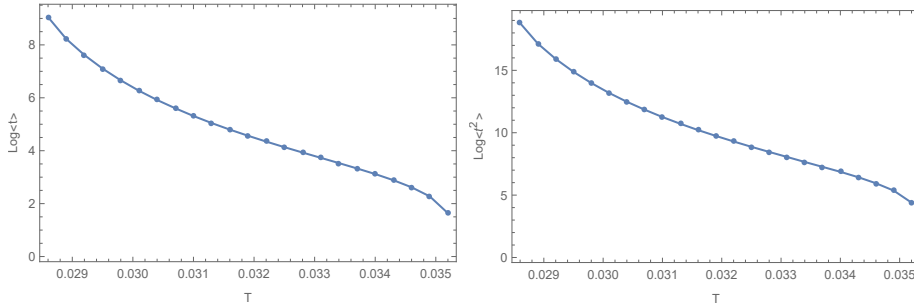


Figure 9. The left panel is the plot of mean first passage time $\langle t \rangle$ from small to large black hole state transition as a function of temperature T and the right is the second order moment of the first passage time distribution $\langle t^2 \rangle$ from small to large black hole state transition. The initial distribution is Gaussian wave packet located at the small black hole state.

fluctuation. The mean first passage time is defined by

$$\langle t \rangle = \int_0^{+\infty} t F_P(t) dt . \quad (4.4)$$

In principle, we can also calculate the n -th moment of time distribution function of first passage time by the relation

$$\langle t^n \rangle = \int_0^{+\infty} t^n F_P(t) dt . \quad (4.5)$$

The mean first passage time $\langle t \rangle$ from small to large black hole state transition and the second order moment of time distribution $\langle t^2 \rangle$ are plotted as a function of temperature T in Fig.9. Note that the vertical axis is in the logarithmic scale. The mean first passage time from the small black hole state to the large black hole state is a monotonic decreasing function of temperature. There are two reasons for this behavior. The first one is that the barrier height from the small black hole state to the large black hole state through the intermediate transition state becomes smaller. Although the thermodynamic stability is determined by the free energy of the black hole state, the kinetics is determined by the barrier height between from the small black hole state to the large black hole state through the intermediate transition state. The second reason is due to the temperature since the thermal diffusion process becomes more effective at higher temperatures.

The fluctuations and relative fluctuations of first passage time are depicted in Fig.10. It can be seen fluctuations will decrease when the temperature increases. This behavior is consistent with the distributions of first passage time displayed in Fig.7, where the peak becomes sharper at higher temperatures. The relative fluctuations decrease firstly when the temperature increases, and attain a minimum at the temperature $T \approx 0.033$. Then the relative fluctuations begin to increase with the temperature. It is obvious that the relative fluctuations attain the maximum at the temperature where the mean first time is at its minimum. We believe that the behavior of the relative fluctuations of the first passage time is the consequence of the two elements mentioned above. As the temperature increases, the free energy barrier height becomes smaller while the temperature becomes higher.

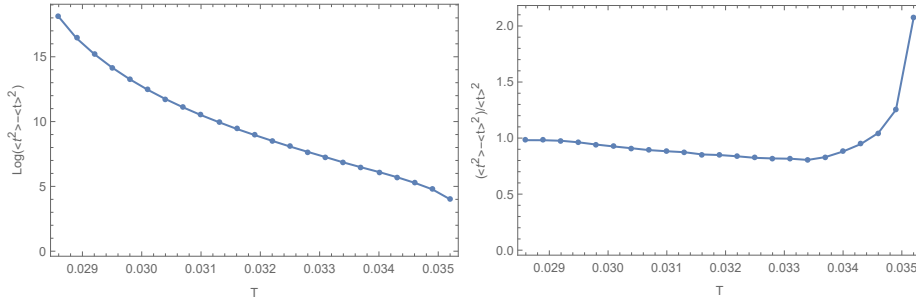


Figure 10. The left panel is the plot of fluctuation $\langle t^2 \rangle - \langle t \rangle^2$ as a function of temperature T and the right is the relative fluctuation $(\langle t^2 \rangle - \langle t \rangle^2) / \langle t \rangle^2$. The initial distribution is Gaussian wave packet located at the small black hole state.

The higher thermal fluctuations relative to the barrier height indicate that the thermal fluctuations will have more significant impacts on the kinetics and associated fluctuations than the free energy barrier height at high temperatures. Therefore, the larger thermal fluctuations relative to the free energy barrier height lead to larger relative fluctuations in kinetics at high temperatures. At last, it can be concluded that the effect of temperature dominates.

At last, we will discuss the first passage kinetic process from large black hole to small black hole. This time the time distribution of first passage process is given by

$$F_p(t) = D \frac{\partial}{\partial r} \rho(r, t) \Big|_{r=r_m}, \quad (4.6)$$

where we impose the reflecting boundary condition at $r = +\infty$ and the absorbing boundary condition at $r = r_m$ (transition state at the free energy barrier top). By numerically solving Fokker-Planck equation with the initial condition and boundary conditions, we can also get the time distributions of first passage process from the large black hole to the small black hole.

In Fig.11, we display the time distribution of first passage process from large black hole to small black hole at different temperatures. It should be noted that when temperature increases the barrier height from the large black hole to the small black hole on the free energy landscape becomes significantly higher as observed from Fig.3. It takes the large black hole state extremely long time to complete the first passage kinetic process of switching the small black hole state on average. It is often difficult to simulate the Fokker-Planck equation for such a long time and to control the numerical error. Therefore, we performed the numerical computations from $T = 0.0286$ to $T = 0.032$. It can be observed that there are also a single peak and an exponential decay tail in every time distribution plot. When the temperature increases, the peak becomes wider. We also show the tail parts of time distributions of first passage process from large black hole to small black hole in one panel in Fig.12. It can be seen the fluctuation will become bigger when increasing temperature.

The mean $\langle t \rangle$ and the second order moment of time distribution $\langle t^2 \rangle$ of the first passage kinetic process switching from the large black hole to the small black hole are plotted as a function of temperature T in Fig.13. In this case, the mean first passage time is a

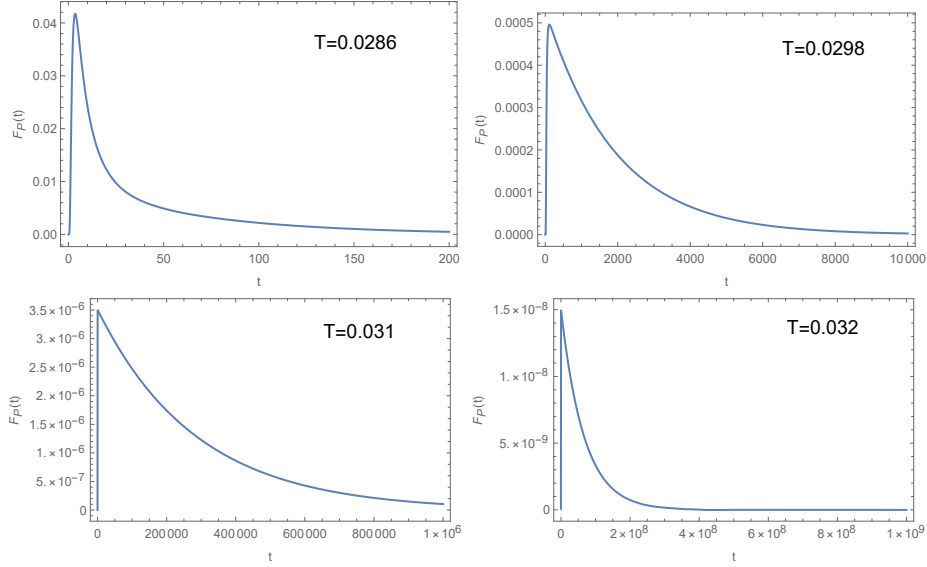


Figure 11. The distributions of first passage time $F_p(t)$ at different temperatures. The initial distribution is Gaussian wave packet located at the large black hole state.

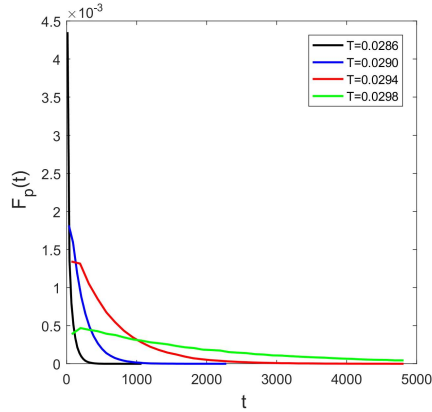


Figure 12. The tail parts of time distributions $F_p(t)$ from large black hole to small black hole at different temperatures.

monotonic increasing function of temperature. For high temperature, the mean first passage time becomes very long. This implies that it is very difficult for the large black hole to escape to the small black hole state. We can conclude that the free energy barrier is the dominant factor that impacts the mean time of the first passage kinetic process of switching from the large black hole to the small black hole.

The fluctuations of the first passage time from the large black hole to the small black hole are depicted in the left panel of Fig.14. It can be seen fluctuations increase with temperature. This behavior is also consistent with the distributions of first passage time displayed in Fig.11, where the peak becomes wider at high temperatures. The behavior of relative fluctuation is plotted in the right panel of Fig.14. The relative fluctuations

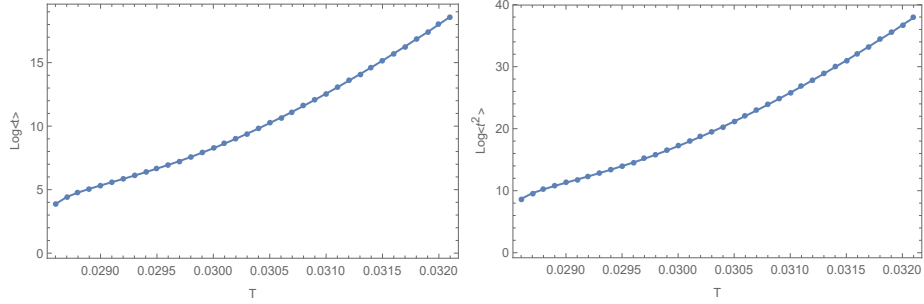


Figure 13. The left panel is the plot of mean first passage time $\langle t \rangle$ from large black hole to small black hole as a function of temperature T and the right is the second order moment of time distribution $\langle t^2 \rangle$. The initial distribution is Gaussian wave packet located at the large black hole state.

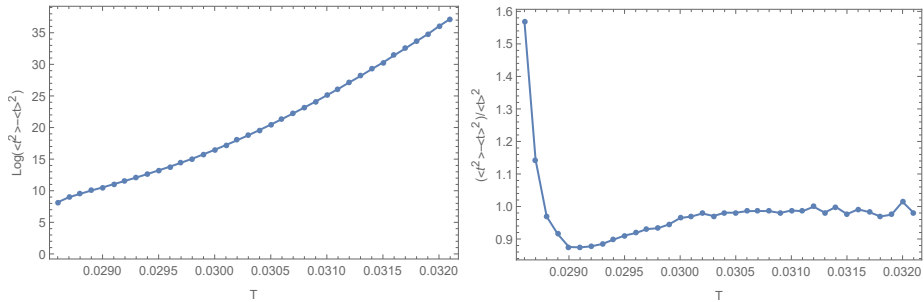


Figure 14. The left panel is the plot of fluctuation $\langle t^2 \rangle - \langle t \rangle^2$ as a function of temperature T and the right is the relative fluctuation $(\langle t^2 \rangle - \langle t \rangle^2) / \langle t \rangle^2$. The initial distribution is Gaussian wave packet located at the small black hole state.

attain the maximum at the temperature where the mean first time is at its minimum. The conclusion is unchanged in this case. As the temperature decreases, the free energy barrier height relative to the temperature decreases. The higher thermal fluctuations relative to the barrier height illustrate that the thermal fluctuations will have more significant impacts on the kinetics and associated fluctuations than the free energy barrier height at low temperatures. Therefore, the larger thermal fluctuations relative to the free energy barrier height lead to larger relative fluctuations in kinetics at low temperatures. As the temperature increases, the relative fluctuations rapidly decrease from the maximum to the minimum, and then increase slowly. It should be pointed out that, because of the considerable numerical errors at high temperature, it is difficult to compute the relative fluctuation precisely.

5 Conclusion

In summary, we have studied the van der waals type phase transition in RNAdS black holes from the viewpoint of free energy landscape. Black holes are considered as thermodynamic entity. We take RNAdS black holes as a macroscopic emergent state in the extended phase space. Phase diagram show the emergent phases of small and large black holes as well as the

coexistence of the small and large black hole as well as the corresponding phase transitions and associated thermodynamic stabilities. Under thermal dynamic fluctuations, there is a chance for switching from one black hole state to another. The mean first passage time for kinetic switching can be related to the life time of the black hole state. In this spirit, we mainly study the Fokker-Planck equation for the state probability evolution in time on the Gibbs free energy landscape of RNAdS black hole. Then we numerically solve the Fokker-Planck equation and obtain the probability distribution of states and time distribution of first passage kinetic process of black hole state switching.

There are still unsolved issues. In the present work, the effect of Hawking radiation is not taken into account. Therefore, it is natural to consider the effect of Hawking radiation on the stochastic thermal dynamic phase transition of RNAdS black holes. The second one is how to relate the first passage time or switching time to the real life time or the stability of the black hole. This study can help to establish a concrete foundation of studying black hole phase transition from stochastic dynamics viewpoint. At last, the interpretation of the van der Waals type phase transition in RNAdS black holes from the holographic duality viewpoint is still missing in the literature. These questions deserve future studies.

Acknowledgement

R. L. would like to thank Dr. Wufu Shi for useful discussion.

References

- [1] S. W. Hawking, Particle creation by black holes, *Commun. Math. Phys.* **43**, 199 (1975).
- [2] P. Hut, Charged black holes and phase transitions, *Mon. Not. R. Astron. Soc.* **180**, 379 (1977).
- [3] P. C. W. Davies, Thermodynamics of black holes, *Rep. Prog. Phys.* **41**, 1313 (1978).
- [4] S. W. Hawking, and D. N. Page, Thermodynamics of black holes in anti-de Sitter space, *Comm. Math. Phys.* **87**, 577 (1982).
- [5] A. Chamblin, R. Emparan, C. Johnson, and R. Myers, Charged AdS black holes and catastrophic holography, *Phys. Rev. D* **60**, 064018 (1999).
- [6] A. Chamblin, R. Emparan, C. Johnson, and R. Myers, Holography, thermodynamics and fluctuations of charged AdS black holes, *Phys. Rev. D* **60**, 104026,(1999).
- [7] X. N. Wu, Multicritical phenomena of Reissner-Nordström anti-de Sitter black holes, *Phys. Rev. D* **62**, 124023,(2000).
- [8] B. Dolan, The cosmological constant and the black hole equation of state, *Class. Quant. Grav.* **28**, 125020 (2011).
- [9] B. P. Dolan, Pressure and volume in the first law of black hole thermodynamics, *Class. Quant. Grav.* **28**, 235017 (2011).
- [10] D. Kubiznak and R. B. Mann, P-V criticality of charged AdS black holes, *J. High Energy Phys.* **1207**, 033 (2012).

- [11] J. M. Maldacena, The large- N limit of superconformal field theories and supergravity, *Adv. Theor. Math. Phys.* **2**, 231 (1998).
- [12] S. S. Gubser, I. R. Klebanov, and A. M. Polyakov, Gauge theory correlators from non-critical string theory, *Phys. Lett. B* **428**, 105 (1998).
- [13] E. Witten, Anti-de Sitter space and holography, *Adv. Theor. Math. Phys.* **2**, 253 (1998).
- [14] E. Witten, Anti-de Sitter Space, thermal phase transition, and confinement in gauge theories, *Adv. Theor. Math. Phys.* **2**, 505 (1998)
- [15] R. G. Cai, L. M. Cao, L. Li, and R. Q. Yang, P-V criticality in the extended phase space of Gauss-Bonnet black holes in AdS space, *J. High Energy Phys.* **1309**, 005 (2013).
- [16] S. W. Wei, and Y. X. Liu, Critical phenomena and thermodynamic geometry of charged Gauss-Bonnet AdS black holes, *Phys. Rev. D* **87**, 044014 (2013).
- [17] D. C. Zou, S. J. Zhang, and B. Wang, Critical behavior of Born-Infeld AdS black holes in the extended phase space thermodynamics, *Phys. Rev. D* **89**, 044002 (2014).
- [18] A. Rajagopal, D. Kubiznak, and R. B. Mann, Van der Waals black hole, *Phys. Lett. B* **737**, 277 (2014).
- [19] J. X. Mo, and W. B. Liu, P-V criticality of topological black holes in Lovelock-Born-Infeld gravity, *Eur. Phys. J. C* **74**, 2836 (2014).
- [20] J. Xu, L. M. Cao, and Y. P. Hu, P-V criticality in the extended phase space of black holes in massive gravity, *Phys. Rev. D* **91**, 124033 (2015).
- [21] S. Fernando, P-V criticality in AdS black hole of massive gravity, *Phys. Rev. D* **94**, 124049 (2016).
- [22] H. Yazdikarimi, A. Sheykhi and Z. Dayyani, Critical behavior of Gauss-Bonnet black holes via an alternative phase space, *Phys. Rev. D* **99**, 124017 (2019).
- [23] A. Dehyadegari, B. R. Majhi, A. Sheykhi and A. Montakhab, Universality class of alternative phase space and Van der Waals criticality, *Phys. Lett. B* **791**, 30 (2019).
- [24] Z. Dayyani, A. Sheykhi, M. H. Dehghani and S. Hajkhalili, Critical behavior and phase transition of dilaton black holes with nonlinear electrodynamics, *Eur. Phys. J. C* **78**, 152 (2018).
- [25] A. Dehyadegari, A. Sheykhi and A. Montakhab, Critical behavior and microscopic structure of charged AdS black holes via an alternative phase space, *Phys. Lett. B* **768**, 235 (2017).
- [26] E. Spallucci, and A. Smailagic, Maxwell's equal area law for charged Anti-deSitter black holes, *Phys. Lett. B* **723**, 436 (2013).
- [27] S. Q. Lan, J. X. Mo, and W. B. Liu, A note on Maxwell's equal area law for black hole phase transition, *Eur. Phys. J. C* **75**, 419 (2015).
- [28] Y. Liu, D. C. Zou, and B. Wang, Signature of the Van der Waals like small-large charged AdS black hole phase transition in quasinormal modes, *J. High Energy Phys.* **1409**, 179 (2014).
- [29] X. X. Zeng, and L. F. Li, Van der Waals phase transition in the framework of holography, *Phys. Lett. B* **764**, 100 (2017).
- [30] S. L. Li, and H. Wei, Holographic entanglement entropy and van der waals transitions in Einstein-Maxwell-Dilaton theory, *Phys. Rev. D* **99**, 064002 (2019).

- [31] D. Astefanesei, R. B. Mann, and R. Rojas, Hairy black hole chemistry, *J. High Energy Phys.* **1911**, 043 (2019).
- [32] M. Kord Zangeneh, A. Dehyadegari, M. R. Mehdizadeh, B. Wang and A. Sheykhi, Thermodynamics, phase transitions and Ruppeiner geometry for Einstein-Dilaton-Lifshitz black holes in the presence of Maxwell and Born-Infeld electrodynamics, *Eur. Phys. J. C* **77**, 423 (2017).
- [33] A. Sahay, Restricted thermodynamic fluctuations and the Ruppeiner geometry of black holes, *Phys. Rev. D* **95**, 064002 (2017).
- [34] S. W. Wei, Y. X. Liu, and R. B. Mann, Ruppeiner geometry, phase transitions, and the microstructure of charged AdS black holes, *Phys. Rev. D* **100**, 124033 (2019).
- [35] Z. M. Xu, B. Wu, and W. L. Yang, Ruppeiner thermodynamic geometry for the Schwarzschild-AdS black hole, *Phys. Rev. D* **101**, 024018 (2020).
- [36] A. Ghosh, and C. Bhamidipati, Contact Geometry and Thermodynamics of Black Holes in AdS Spacetimes *Phys. Rev. D* **100**, 126020 (2019).
- [37] S. W. Wei, and Y. X. Liu, Insight into the microscopic structure of an AdS black hole from a thermodynamical phase transition, *Phys. Rev. Lett.* **115**, 111302(2015); Erratum: *Phys. Rev. Lett.* **116**, 169903 (2016).
- [38] S. W. Wei, Y. X. Liu, and R. B. Mann, Repulsive Interactions and Universal Properties of Charged Anti-de Sitter Black Hole Microstructures *Phys. Rev. Lett.* **123**, 071103 (2019).
- [39] D. Kubiznak, R. B. Mann, and M. Teo, Black hole chemistry: thermodynamics with Lambda, *Class. Quant. Grav.* **34**, 063001 (2017).
- [40] N. Goldenfeld, *Lectures on Phase Transitions and the Renormalization Group* (Westview Press, Boulder, 1992)
- [41] H. Frauenfelder, S. G. Sligar, and P. G. Wolynes, The energy landscapes and motions of proteins, *Science* **254**, 1598 (1991).
- [42] H. Frauenfelder and P. G. Wolynes, Biomolecules: Where the physics of complexity and simplicity meet, *Phys. Today* **2**, **47**, 58 (1994).
- [43] R. Li, and J. Wang, Thermodynamics and kinetics of Hawking-Page phase transition, *Phys. Rev. D* **102**, 024085 (2020).
- [44] R. Zwanzig, *Nonequilibrium Statistical Mechanics*, Oxford University Press (2001).
- [45] C.-L. Lee, C.-T. Lin, G. Stell, and J. Wang, Diffusion dynamics, moments, and distribution of first-passage time on the protein-folding energy landscape, with applications to single molecules, *Phys. Rev. E* **67**, 041905 (2003).
- [46] C.-L. Lee, G. Stell, and J. Wang, First-passage time distribution and non-Markovian diffusion dynamics of protein folding, *J. Chem. Phys.* **118**, 959 (2003).
- [47] J. Wang, Landscape and flux theory of non-equilibrium dynamical systems with application to biology, *Advances in Physics*, **64**, 1 (2015).
- [48] J. D. Bryngelson, and P. G. Wolynes, Intermediates and Barrier Crossing in a Random Energy Model (with Applications to Protein Folding), *J. Phys. Chem.* **93**, 6902 (1989).
- [49] S. W. Wei, Y. X. Liu and R. B. Mann, Ruppeiner Geometry, Phase Transitions, and the Microstructure of Charged AdS Black Holes, *Phys. Rev. D* **100**, 124033 (2019).

- [50] S. W. Wei and Y. X. Liu, Intriguing microstructures of five-dimensional neutral Gauss-Bonnet AdS black hole, *Phys. Lett. B* **803**, 135287 (2020).
- [51] A. Ghosh and C. Bhamidipati, Thermodynamic geometry and interacting microstructures of BTZ black holes, *Phys. Rev. D* **101**, 106007 (2020).
- [52] P. K. Yerra and C. Bhamidipati, Ruppeiner Geometry, Phase Transitions and Microstructures of Black Holes in Massive Gravity, [arXiv:2006.07775 [hep-th]].
- [53] A. Dehyadegari, A. Sheykhi and S. W. Wei, Microstructure of charged AdS black hole via $P - V$ criticality, [arXiv:2006.12265 [gr-qc]].
- [54] A. Sheykhi, M. Arab, Z. Dayyani and A. Dehyadegari, Alternative approach towards critical behavior and microscopic structure of the higher dimensional Power-Maxwell black holes, *Phys. Rev. D* **101**, 064019 (2020).
- [55] B. Carter, *Black Holes*, edited by C. M. DeWitt and B. S. DeWitt (Gordon and Breach, New York, 1973).
- [56] J. W. York, Black hole thermodynamics and the Euclidean Einstein action, *Phys. Rev. D* **33**, 2092 (1986).
- [57] R. Andre, and J. P. S. Lemos, Thermodynamics of five-dimensional Schwarzschild black holes in the canonical ensemble, *Phys. Rev. D* **102**, 024006 (2020).